ORIGINAL ARTICLE

Study on seismic performance of high-strength steel earthquake-resilient beam-column joint with double damage elements

Hongchao Guo[a, b, *], Dongdong Zheng[b], Jing Lu[b], Xudong Zhou[b], Wenqi Wang[b], Yunhe Liu[a]

[a] State Key Laboratory of Eco-hydraulics in Northwest Arid Region of China, Xi'an University of Technology, No.5 Jinhua Road, Xi'an 710048, PR China
[b] School of Civil Engineering and Architecture, Xi'an University of Technology, No.5 Jinhua Road, Xi'an 710048, PR China
*Corresponding Author: Hongchao Guo. Email: ghc-1209@163.com

Abstract: The mutual constraint between bearing capacity, stiffness, and post earthquake recoverability has always been the contradiction of earthquake resilient joint. Taking into account the above three factors, this paper proposes a high-strength steel earthquake resilient beam column joint with double damage elements. Low cycle reciprocating loading tests were conducted, and a refined finite element model was established for parameter expansion analysis. The research findings show a significant time sequence in the joint double damage element, with both components dissipating over 90% of energy. In contrast, main components like beams and columns dissipate less than 10% of energy. The residual deformation of the joints is within the specified DS2 level limit in the FEAM P-58 standard, indicating excellent post-earthquake recoverable performance. The influence of the length l_b of the energy dissipation section in the middle of the flange cover plate, the height h_s of the stiffening rib, the length l_c of the cantilever beam, and the cutting angle α_a of the butterfly damper on the joint performance was studied. The results show that l_b significantly affects the loading stability of the flange cover plate, thereby affecting the joint performance. It is recommended to ensure that the stability coefficient of the flange cover plate is not less than 0.967; Considering all factors, it is recommended that h_s be taken as 0.2 times the width of the flange cover plate, l_c be taken as 1.3 times the height of the beam, and α_a taken as 50°. Finally, a calculation method for the joint trilinear skeleton curve model was proposed through theoretical derivation and data fitting. By comparing the theoretical calculation results with experimental and finite element calculation results, it was found that the curves matched well, proving the effectiveness of the proposed joint skeleton curve calculation method.

Keywords: Double damage element, high strength steel, post-earthquake recovery performance evaluation, repairable threshold

1 Introduction

The seismic resistance of building structures has been a major focus in the field of structural engineering. After the Northridge Earthquake in the United States and the Kobe earthquake in Japan [1, 2], it was discovered that the main failure mode of steel structures during earthquakes is the premature cracking of welds at beam column connections. This has been identified as the primary factor limiting the seismic performance of steel structures. Scholars have suggested several methods to improve this.

These methods can be divided into two types. The first type involves deliberately weakening the beam flange and web area. During an earthquake, this weakened area experiences damage first, forming plastic hinges. This helps prevent weld cracking in the connection area of beam column joints and significantly increases the ductility of the structure. The most common forms of weakening include dog bone weakening [3], tapered weakening [4, 5], and beam web opening weakening [6, 7]. Another method to strengthen the connection area between beams and columns. Common strengthening techniques include plate connection strengthening [8] and flange transition strengthening [9]. Compared to weakened connections, this type of connection not only allows for plastic hinge outward movement but also has a higher load carrying capacity. Therefore, it is more commonly used in engineering.

The structure described above addresses the issue of brittle cracking at the connection points between steel structure beams and columns during earthquakes. This significantly enhances the seismic performance of the joints. When considering the entire earthquake cycle, it's important to note that the structure will sustain irreversible damage and deformation after an earthquake, making repairs challenging. As a result, demolition and reconstruction would lead to substantial economic waste. The post earthquake functional recovery structure will help solve the above problems. Zhang and Jiang [10, 11] proposed a flange cover plate connection beam column joint, which can achieve post earthquake functional recovery by replacing the flange cover plate; Francavilla [12] proposed a friction type connection joint that connects damage elements with beams and columns through Belleville disk springs, significantly improving the energy dissipation performance of the joint. Jiao [13] proposed a beam column joint with T-shaped energy dissipation device connected by plastic hinges. The T-shaped energy dissipation device increases its cross-sectional moment of inertia, which helps to enhance the load-bearing capacity of the joint. Men [14] proposed beam column joints with replaceable T-shaped connectors. Through experimental research, it has been found that T-shaped connectors can consume over 90% of energy during earthquakes, thereby protecting the main components of beams and columns. Xu [15] combined the advantages of prefabricated structures with earthquake resilient structures and proposed a modular self-centering joint. After experimentation, it was found that the nodes have high bearing capacity and low residual deformation. Liu [16] proposed a beam column joint form that combines energy dissipation through deformation of the flange cover plate and friction of the web slot, enriching the energy dissipation mechanism of the joint and improving its performance. The premature buckling deformation of the flange cover plate is a key factor affecting the performance of the joint. Xu [17] proposed a joint form with a buckling restrained plate and a core plate energy dissipation component, which solved the problem of premature buckling of the flange cover plate and improved the joint performance. From the perspective of damaged materials, selecting different types of steel can also improve structural performance. Wang [18] used low yield point steel damage elements for joint design. Low yield point steels have a better plastic deformation capacity than ordinary steels, which can significantly increase structural energy consumption, but have a lower loading capacity. Tong [19] proposed the joint of cast steel connectors. The experimental results indicate that, when compared to regular low-carbon steel joints, this joint exhibits less significant strength degradation in the later stage and has a more stable bearing capacity. However, it comes at a higher cost and is less commonly used in engineering applications. Overall, regular low-carbon steel remains the optimal choice as a structural damage element.

It is important to evaluate the performance of earthquake resilient joints after an earthquake to ensure they can function properly. Currently, the method for evaluating post-earthquake recoverability in earthquake resilient joints involves loading the joints to the ultimate failure stage, replacing the damaged components, and then loading them again. Because of the unpredictable nature of earthquakes, structures may not behave as expected when they reach their maximum load capacity. In such cases, the residual displacement of the structure is significantly higher than the threshold for repairable displacement [20-22]. Therefore, replacing the damaged elements may not be very effective. This article examines the current seismic system and compares the specifications of AISC 341-16 [23], EN 1998-1 [24], and FEMA-267 [25]. The displacement angle for joint replacement is set at an ultimate rotation angle of 0.04 rad for high ductility steel structures. Following replacement, the joints are reloaded until failure, and the structure's post-earthquake recovery performance is assessed.

Based on the research background provided, this paper proposes a high-strength steel earthquake resilient beam-column joint with double damage elements to achieve excellent load-bearing, energy

dissipation, stiffness, and post-earthquake recoverability. The assembly steps are illustrated in **Fig. 1**. Normal steel is chosen as the replaceable damage element for energy dissipation, and high strength steel is used as the main structure of the beam-column to withstand the external loads. This design allows the joint to have the same bearing capacity and energy dissipation capacity as normal steel joints, while also providing the joint with the ability to recover after an earthquake. Due to the higher strength and elastic strain of high-strength steel compared to ordinary steel, a double damage element design with flange cover plates and butterfly dampers is adopted to fully utilize the advantages of high-strength steel. During the loading process, the flange cover plate provides the bending bearing capacity of the joint through tensile and compressive deformation, while the butterfly damper carries out bearing and energy dissipation through bending-shear composite deformation, enriching the joint bearing and energy dissipation mechanism. The flange cover plate and butterfly damper are placed at the positions of the beam flange and web. This helps to disperse energy dissipation at joints, prevent excessive concentration of plastic deformation on the beam flange, and reduce residual deformation of the joint. Under the dispersed arrangement of damage elements, there is a significant yield time sequence, which increases the safety of joint in the face of aftershocks and earthquake uncertainties. The ear plate is connected by a pin to ensure shear force transmission, becoming a force transmission link between the damaged element and the beam and column. From the perspective of stiffness, the use of artificial plastic hinges avoids cutting damaged components and helps to enhance the lateral stiffness of the structure. Based on the above considerations, this study will focus on the collaborative relationship between joint double damage elements during the loading process, including strain development, energy dissipation, and failure laws, and evaluate the post earthquake recoverable performance of joint; Summarize the impact of key parameters of damage elements on joint performance through parameter extension analysis, summarize the design method of double damage elements. Propose a theoretical calculation model with double damage element joint, in order to provide reference and inspiration for research on similar structures.
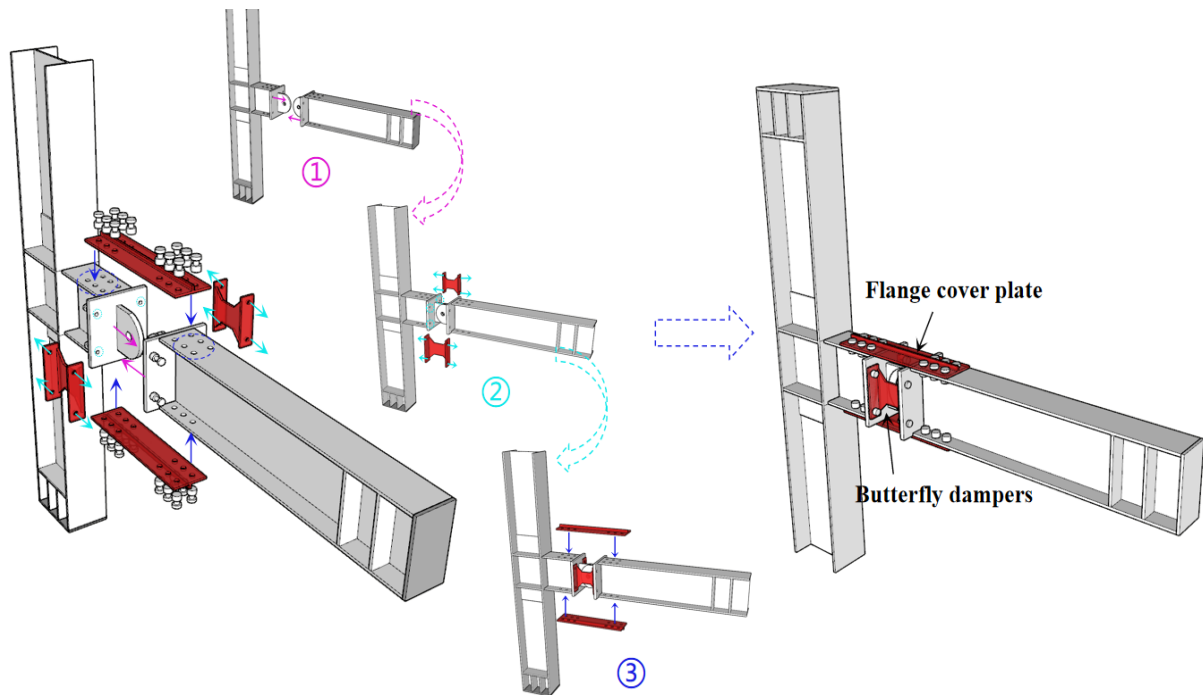

Fig. 1 Beam-column joint

2 Joint design

Three types of joints were designed in total. The beams and columns are made of Q460 high-strength steel. Flange connection plates and butterfly dampers as damage components are made of Q235. Joint number -235 represents the steel grade, DJ is the abbreviation for double damage element joint, and R represents loading the joint to 0.04 rad to replace the damage element; F represents loading the joint to destruction. The specific situation is shown in **Table 1**, and the joint size is shown in **Fig. 2**.

Table 1. Joint design

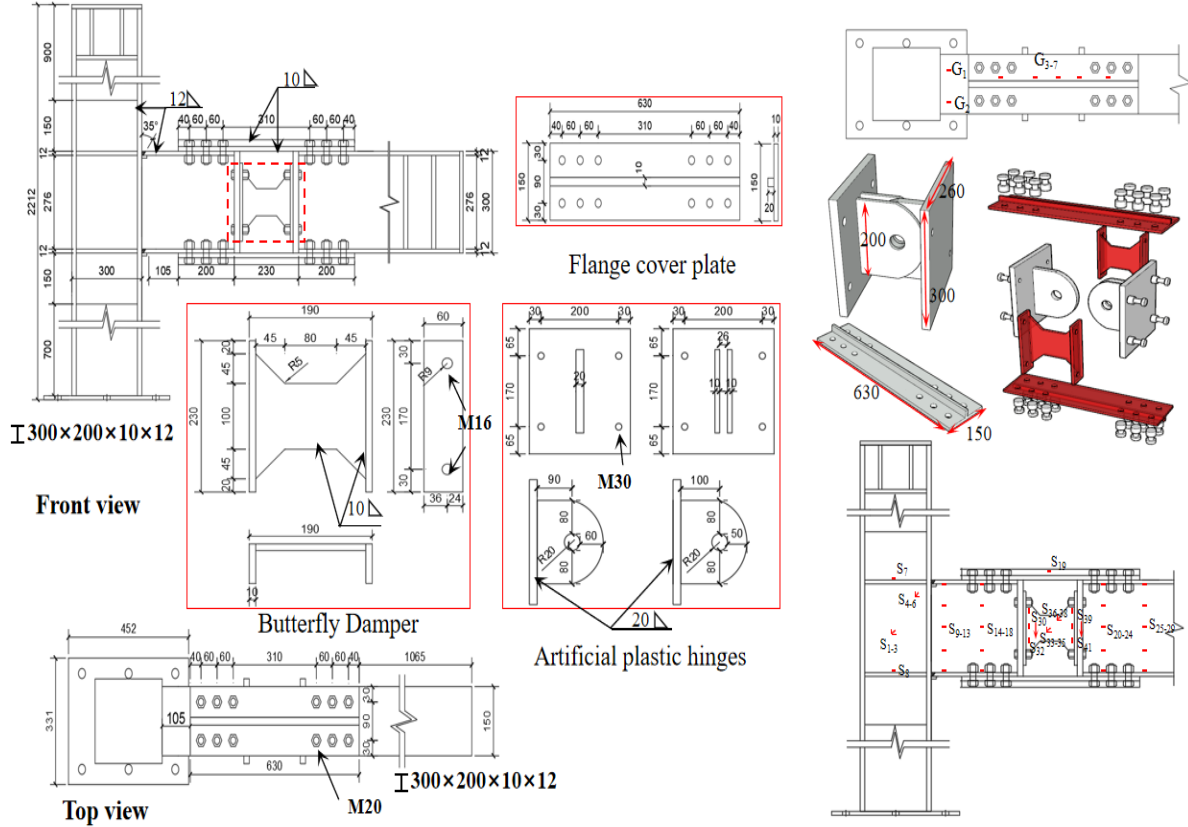| Specimens	Beam cross-section size (mm)	Column cross-section size (mm)	Replaceable element	Loading system
DJR-235				Load to 0.04 rad, replace **[AISC 341-16]**
DJF-235	H300×150×8×12 (Q460)	H300×200×10×12 (Q460)	Flange cover plate + butterfly damper (Q235)	Load to failure **[AISC 341-10]**
DJF-355			Flange cover plate + butterfly damper (Q355)	Load to failure **[AISC 341-10]**

Fig. 2 Joint size (mm)

3 Specimen loading

3.1 Loading systems

The two ends of the steel column are hinged horizontally on the ground beam. Hydraulic jacks on the east side of the column are used to apply axial pressure, with an axial compression ratio of 0.2 [8]. The east side reaction bearing is connected to the hydraulic jack through 6 M30 high-strength bolts, while the reaction bearing is connected to the ground beam through 8 M30 high-strength bolts. The west side reaction bearing is connected to the column end by articulation. During the loading process, the beam-column joint, the reaction bearing, and the ground beam form a complete self-balancing system. To ensure the accuracy of the test data, two sets of strain acquisition systems are used for mutual verification. One is the VIC-3D non-contact strain acquisition system, and the other is the JM3816 multi-channel strain acquisition system. The steel beam is vertically connected with the steel column, and lateral support is set in the middle of the steel beam to prevent out of plane instability of the beam during loading. Please refer to **Fig. 3 (a)** for details. The MTS actuator is connected to the steel beam to achieve loading of reciprocating horizontal displacement. The experimental loading system refers to the American standard AISC 341-10 [26], as shown in **Fig. 3 (b)**.

(a) Loading device
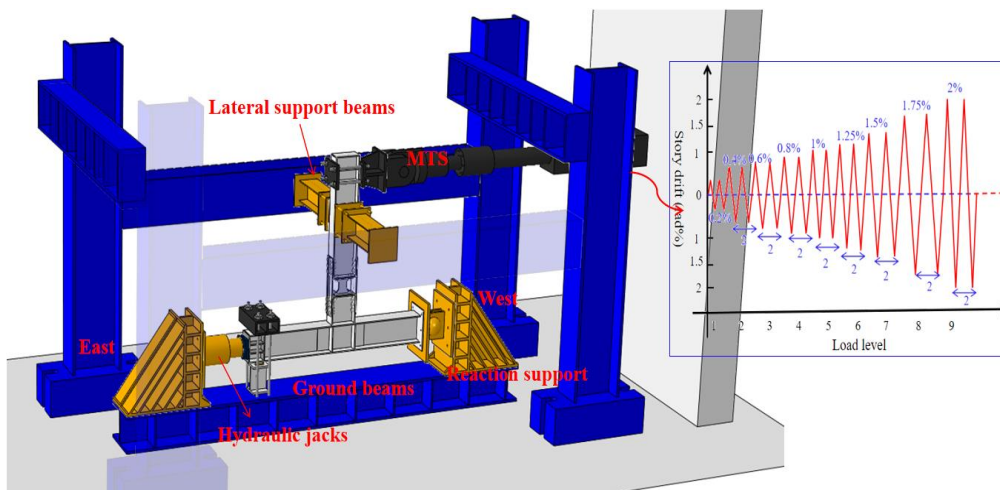
(b) Loading system

Fig. 3 Loading arrangement

3.2 Material Test

In accordance with the "*Metal Materials Tensile Test Method 1 at Room Temperature*" (GB/T228.1-2010) [27], uniaxial tensile tests were performed on the specified steel. The tensile device and test results are illustrated in **Fig. 4,** and detailed performance parameters are provided in **Table 2**.
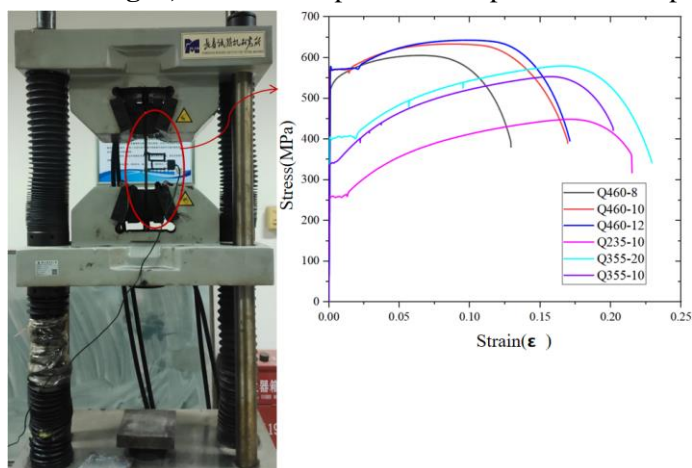

Fig. 4 Monotonic tensile test of steel

Table 2. Material test results

| Tensile specimens	Thickness t/mm	Tield strength f_y / MPa	Ultimate strength f_u / MPa	Modulus of elasticity E_s/ GPa	Elongation δ/%	Flexural ratio f_y/ f_u
Q460-8	8	540.49	657.51	201.1	14.8	0.82
Q460-10	10	570.38	633.48	205.9	17.6	0.90
Q460-12	12	584.99	726.14	203.6	20.0	0.81
Q235-10	10	300	465	203.0	24.0	0.65
Q355-10	10	355	553	206.0	23.2	0.64
Q355-20	20	398	579	206.0	25.8	0.69

## 4 Joint performance

4.1 Damage phenomenon

The damage phenomenon of the specimen is shown in **Fig. 5**. During the whole loading process, the specimen DJR-235 did not have the phenomenon of steel fracture and bolt breakage. When loaded to 0.035rad, the connection plate of the butterfly damper was bent under the bending-shear load, and the bolts were not loosened. Based on the deformation cloud diagram obtained from VIC-3D, it is evident that the butterfly damper experiences bending-shear deformation, with bending deformation being significantly greater than shear deformation. When subjected to a 0.04 rad load, the flange cover plate exhibited slight bending. Additionally, the average residual deformation of the beam-column joint is 0.22%, indicating that the joint maintains good post-earthquake recoverable performance even when it reaches the ultimate angle of the ductile frame structure. When the displacement of specimen DJF-235 reaches 0.02rad, dense stress stripes appear at the corners of the butterfly damper, and the strain there has reached the yield strain. It can be seen from the strain cloud diagram that the butterfly damper is prone to the formation of strain concentration in the position of the cross-section mutation. When the displacement is loaded to 0.04 rad, the flange cover plate undergoes obvious bending deformation. Based on the deformation cloud diagram, we can observe a 4.5mm displacement variance between the left and right sections of the butterfly damper resulting from bending deformation, and a 5.5mm displacement variance between the upper and lower sections due to shear deformation. This suggests that the butterfly damper undergoes bending-shear composite deformation during the loading process. The damage phenomenon of specimen DJF-355 is consistent with DJF-235, and the flange cover plate slips significantly during the loading process. The analysis indicates that as the strength of the flange cover plate increases, the bolt friction under the tensile-pressure bearing mechanism is insufficient to allow the flange cover plate to reach its ultimate strength. The flange cover plate can only reach its ultimate strength when the bolt slips to the bolt rod and the hole wall extrusion occur. The deformation cloud diagram shows that the shear deformation of the butterfly damper in the X-direction is 16mm, and the bending deformation in the Y-direction is approximately 4.35mm. This suggests that the butterfly damper undergoes a combined deformation, with shear deformation being the primary deformation and bending deformation serving as the secondary deformation.
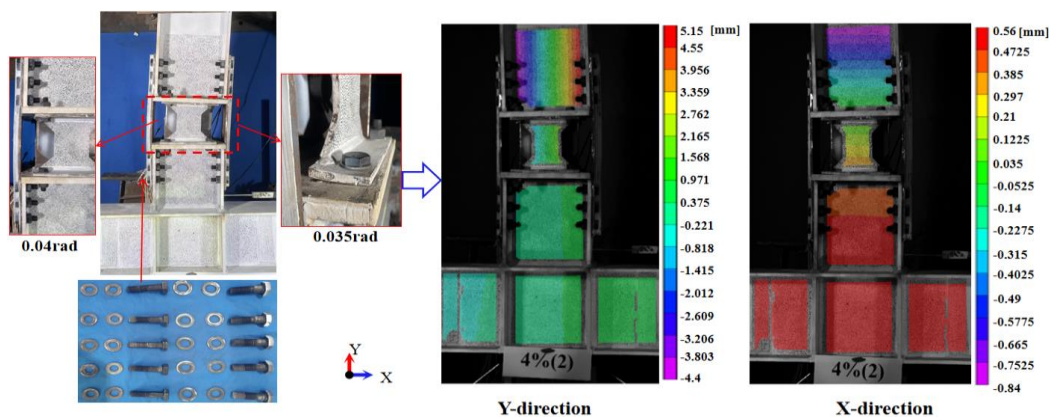
(a) DJR-235
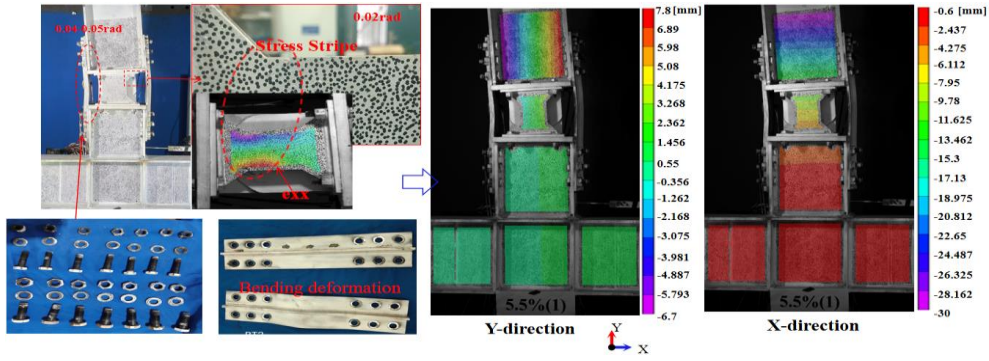
(b) DJF-235
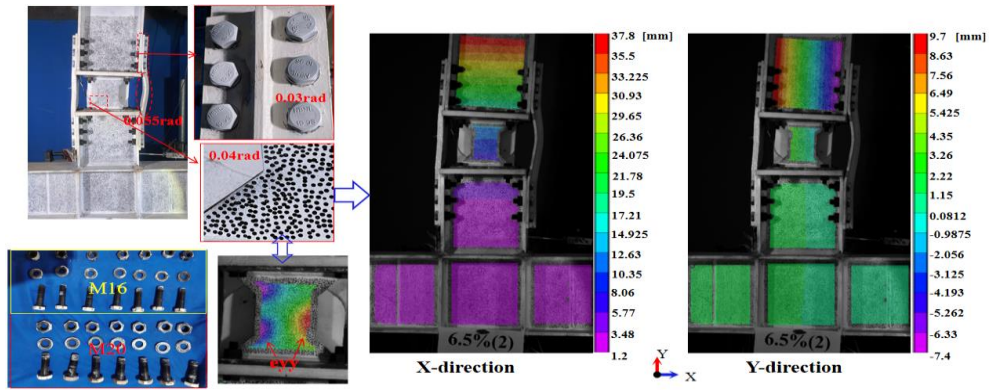
(c) DJF-355

Fig. 5 Phenomenon of damage

4.2 Mechanical property

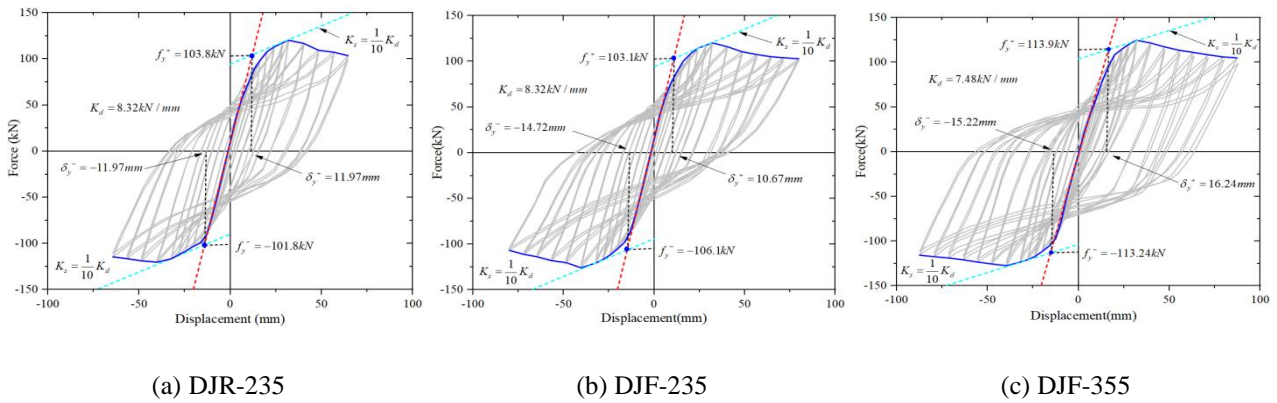(a) DJR-235   (b) DJF-235   (c) DJF-355

Fig. 6 Hysteresis curve

The hysteresis curve of the specimen is depicted in **Fig. 6**. The yield load and displacement of the specimen were determined using the method recommended by ECCS [28], and the mechanical performance parameters are presented in **Table 3**, where K_d represents the initial stiffness, δ_y represents the joint yield displacement, f_y represents the joint yield bearing capacity, f_k represents the joint peak bearing capacity, μ represents the joint ductility coefficient, and E represents the joint energy dissipation. As can be seen from **Table 3**, when the loading displacement reaches 0.04 rad, the peak bearing capacity, ductility, and energy consumption of specimen DJF-235 reached 95.6%, 79.8%, and 72.5% of the ultimate limit state, respectively. After replacing the damaged steel with a higher grade steel, there was no significant change in the peak load carrying capacity and ductility of the joint. The yield load increased by 10.7%, the yield displacement grew by 27%, and the energy dissipation

capacity improved by 54.8%. This indicates that replacing the damaged steel slows down the yielding of the joint and significantly improves the joint's energy dissipation.

Table 3. Mechanical properties parameters of joint

Specimen	K_d (kN/mm)	δ_y^+ (mm)	f_y^+ (kN)	δ_y^- (mm)	f_y^- (kN)	f_k (kN)	μ	E (KJ)
DJR-235	8.32	11.97	103.8	-13.81	-101.8	120.3	5.02	87.6
DJF-235	8.32	10.67	103.1	-14.72	-106.1	125.8	6.29	120.8
DJF-355	7.48	16.24	114	-15.22	-113.24	127.3	6.28	187

4.3 Strain analysis

The VIC-3D strain acquisition system was used to analyze the strain of columns, cantilever beams, flange cover plates, and butterfly dampers. The results are shown in **Fig. 7**. From the figure, it can be observed that during the loading process, the plastic strain is mainly concentrated in the flange cover plates and butterfly dampers, while the beams and columns, as well as other components, remain in the elastic state. The strain is always lower than $1799\mu\varepsilon$, which achieves a centralized and controllable joint damage and a double damage element energy dissipation mechanism. Based on the strain cloud diagrams, it is evident that the double damage elements can work together to withstand forces, and there is a noticeable sequence of yielding between the double damage elements. When the steel grade of the damage element is Q235, the yield displacement of the flange cover plate ranges from 0.01 to 0.015 rad, while the yield displacement of the butterfly damper ranges from 0.01 to 0.02 rad. The yield displacement difference between the flange cover plate and the butterfly damper is in the range of 0 to 0.05 rad. When the steel strength of the damage element is selected Q355, the increase in steel yield strength leads to a significant increase in joint displacement when the flange cover plate yields, which is 0.035 rad. In comparison, the joint displacement when the butterfly damping yields is 0.015 rad. The difference between the two yield displacements is 0.02 rad. This indicates that as the steel strength of the damage element increases, the yielding time sequence between the two damage elements becomes more evident.
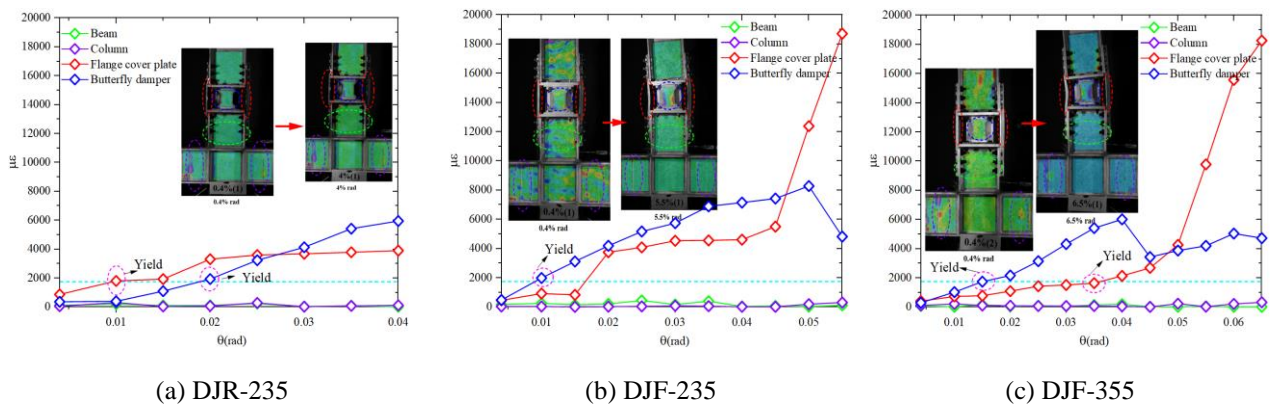

(a) DJR-235   (b) DJF-235   (c) DJF-355

Fig. 7 Strain analysis

4.4 Hysteresis curves for each part of the joint

The hysteresis curves for the beam, panel zone, and columns were obtained using Eq. (1-7) and are displayed in **(Fig. 8, Fig. 9)** shows the schematic of the joint force and the arrangement of displacement gauges. The energy consumption and the percentage of energy consumption in each part of the joint are determined by calculating the area enclosed by the hysteresis curve. In **Fig. 9**, it is evident that the hysteresis curve of the beam section damper in joint DJR-235 is complete, with an energy consumption of 84.45 kN·m, which accounts for 96.4% of the total energy consumption. The columns and panel zone are in the elastic phase, with both having an energy consumption ratio of less than 2%. This indicates that the main components remain elastic when the loading displacement reaches the ductile steel frame criterion. In joint DJF-235, when loaded to damage, the beam segment damper dissipates 95.8% of the energy. At this point, the energy consumption of the column is 3.87 kN·m, accounting for 3.2% of the total energy consumption, and the energy consumption of the panel zone is 0.95%. It's noted that when the joints are under extreme load, the main components can still maintain

their elastic state, and the plastic damage is mainly concentrated in the double damage element. When the steel grade of the damage element is changed from Q235 to Q355, the energy consumption proportion of the beam section damper decreases to 90%, while the energy consumption proportion of the column and panel zone is 6.5% and 3.67%, respectively. When compared to the main components of DJF-235 joint, the energy consumption share of main structural components of DJF-355 increases significantly. However, this proportion remains less than 10%, ensuring that the joint can achieve centralized damage controllability during earthquakes.

(a) Diagram of displacement measurement   (b) Diagram of bearing capacity
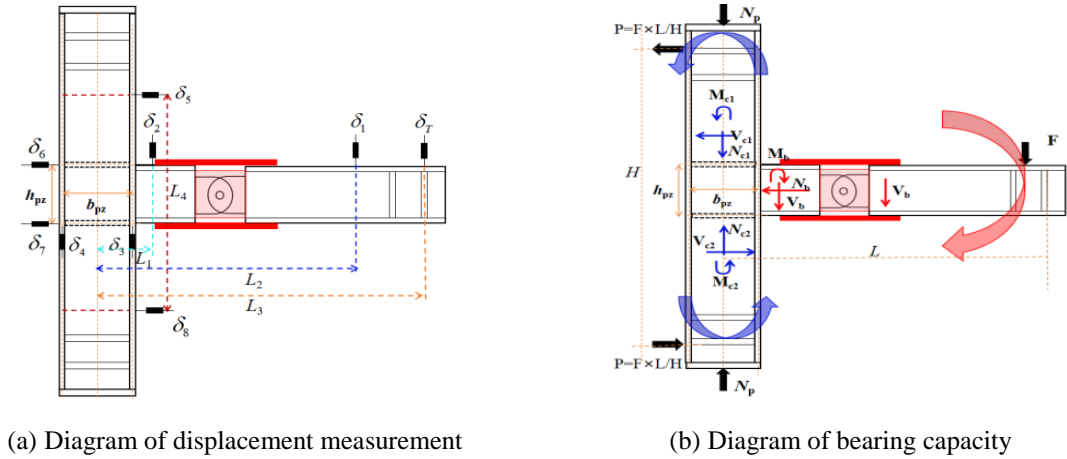
Fig.8 Load and displacement calculation of joint

(a) DJR-235

(b) DJF-235

(c) DJF-355
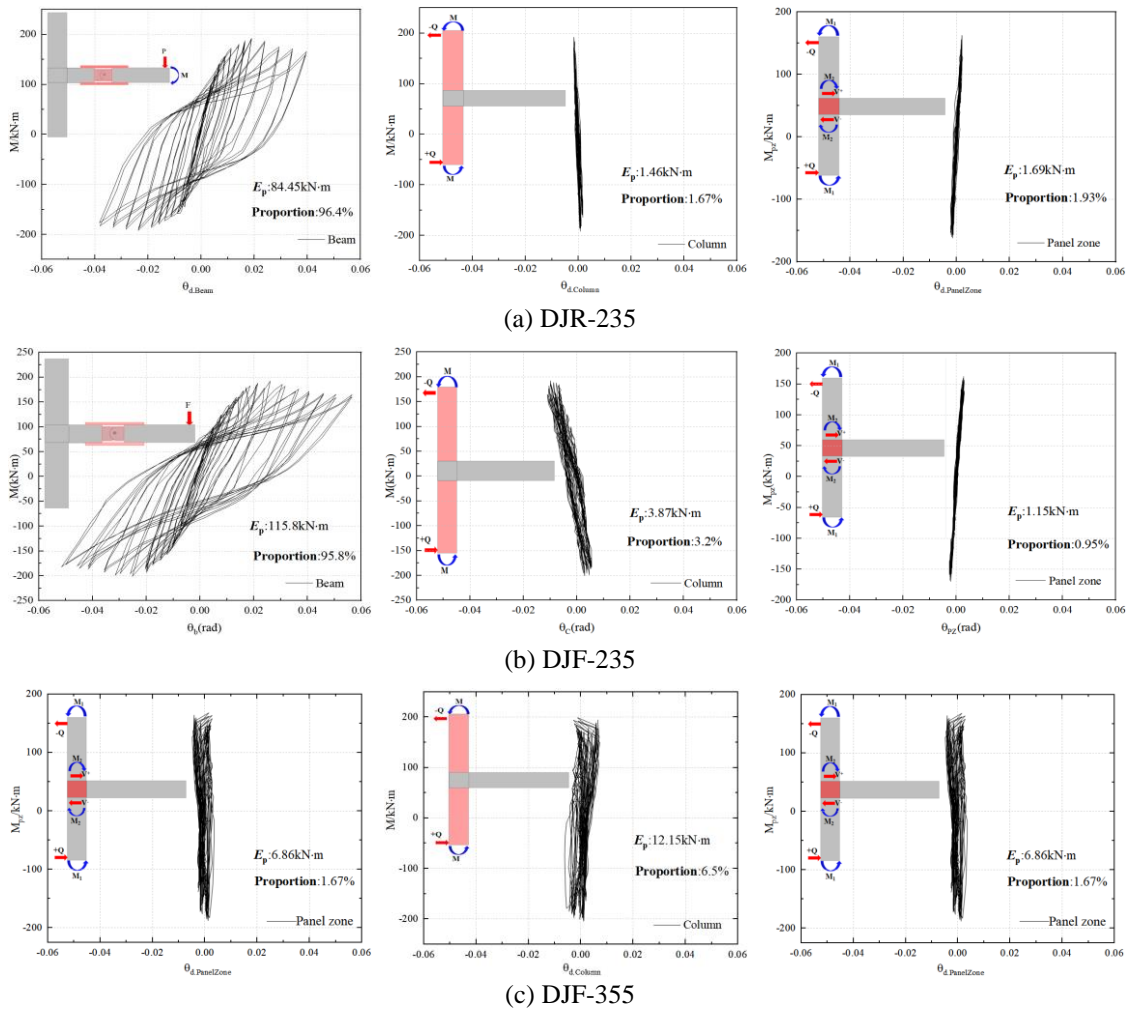
Fig. 9 Hysteresis curves for each part of the joint

$$\theta_d = \frac{\delta_T}{L_3} - \frac{\delta_5 - \delta_8}{L_4} \tag{1}$$

$$M_{pz} = M_b - \left(\frac{V_{c1} + V_{c2}}{2}\right) h_{pz} = F \times L \times \left(1 - \frac{b_{pz}}{2L} - \frac{h_{pz}}{H}\right) \tag{2}$$

$$\theta_{PZ} = \frac{\delta_6 - \delta_7}{h_{pz}} - \frac{\delta_4 - \delta_3}{b_{pz}} \tag{3}$$

$$M_c = P \times H \tag{4}$$

$$\theta_c = \frac{\delta_6 - \delta_7}{h_{pz}} - \frac{\delta_5 - \delta_8}{L_4} - \theta_{PZ} \tag{5}$$

$$M_b = F \times \left(L - \frac{b_{pz}}{2}\right) \tag{6}$$

$$\theta_b = \theta_d - \theta_c - \theta_{PZ} \tag{7}$$

Among them, θ_d is the story drift ratio of the joint, M_{pz}, θ_{pz} are the bending moment and deformation borne by the panel zone, M_c, θ_c are the bending moment and deformation borne by the column, M_b, θ_b are the bending moment load and deformation borne by the beam, respectively. The parameters L_1-L_4, H, L, as well as h_{pz} and b_{pz} are shown in **Fig. 8**.

4.5 Post-earthquake recovery performance evaluation

In evaluating the post-seismic recoverable performance of structures, various methods are used, including statistical repair time, post-seismic residual displacement [29], and comparison of hysteresis curves before and after the replacement of damaged elements [30]. Sections 4.3, 4.4 demonstrate that the joints can be damage-controllable based on strain analysis and the proportion of energy dissipation. In this section, the hysteresis curve comparison reveals that the hysteresis curves before and after damage element replacement are basically the same, see **Fig. 10** for details. It shows that the performance of the joint can be fully recovered after replacing the damage element within the limit angle of the ductile frame. The damage state of steel structures in the FEAM P-58[31] standard is defined based on residual displacement angle, which is divided into four levels: DS1-DS4. When the structure is in DS1 state ($\theta_r \leq 0.002$rad), it can continue to be used without repair. When the structure is in DS2 state, only non-structural components need to be repaired. When in DS4, the structure will lose its repairability. Statistics were conducted on the residual deformation of three types of joints, and the results showed that the maximum residual deformation of all three types of joints was lower than the DS2 specified value, indicating that the nodes have excellent post-earthquake recoverable performance.
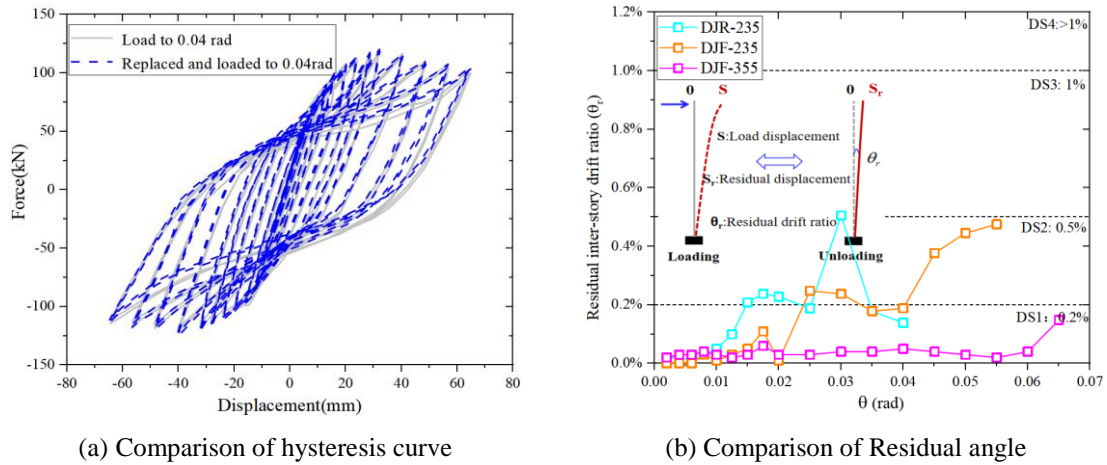

(a) Comparison of hysteresis curve   (b) Comparison of Residual angle

Fig. 10 Post earthquake recoverable performance evaluation

5 Finite element analysis

5.1 Establishment of finite element models

An ABAQUS finite element model was established to analyze the joints. The joints are modeled with C3D8R solid units, and the steel constitutive model is a kinematically strengthened model. This model account for the Bauschinger effect and is suitable for steel simulation under cyclic loading. Tie is used in the contact relationship to simulate welding, and "surface to surface" contact pairs are used to simulate the contact relationship between the flange cover plate and the beam, as well as the contact relationship between the ear plate. The damage element mesh was locally refined for calculation accuracy. The details are shown in **Fig. 11**.
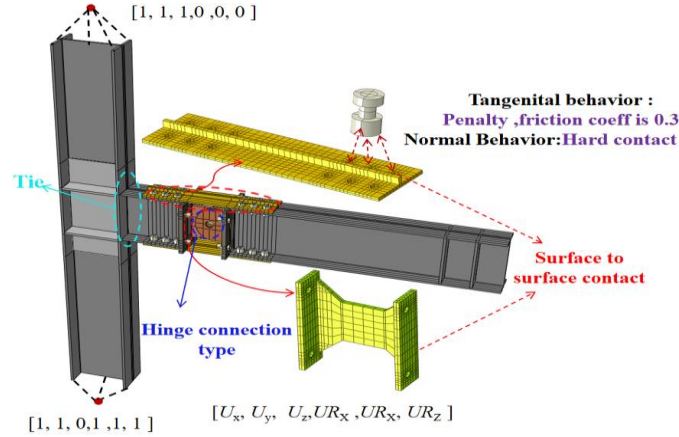
Fig. 11 Finite element model

The model calculation results are compared with the test results to verify the accuracy of the model, and the results are shown in **Fig. 12**. It is evident from the figure that the finite element calculation results are in good agreement with the test results. The model can better reflect the mechanical properties and failure phenomena of the joints.
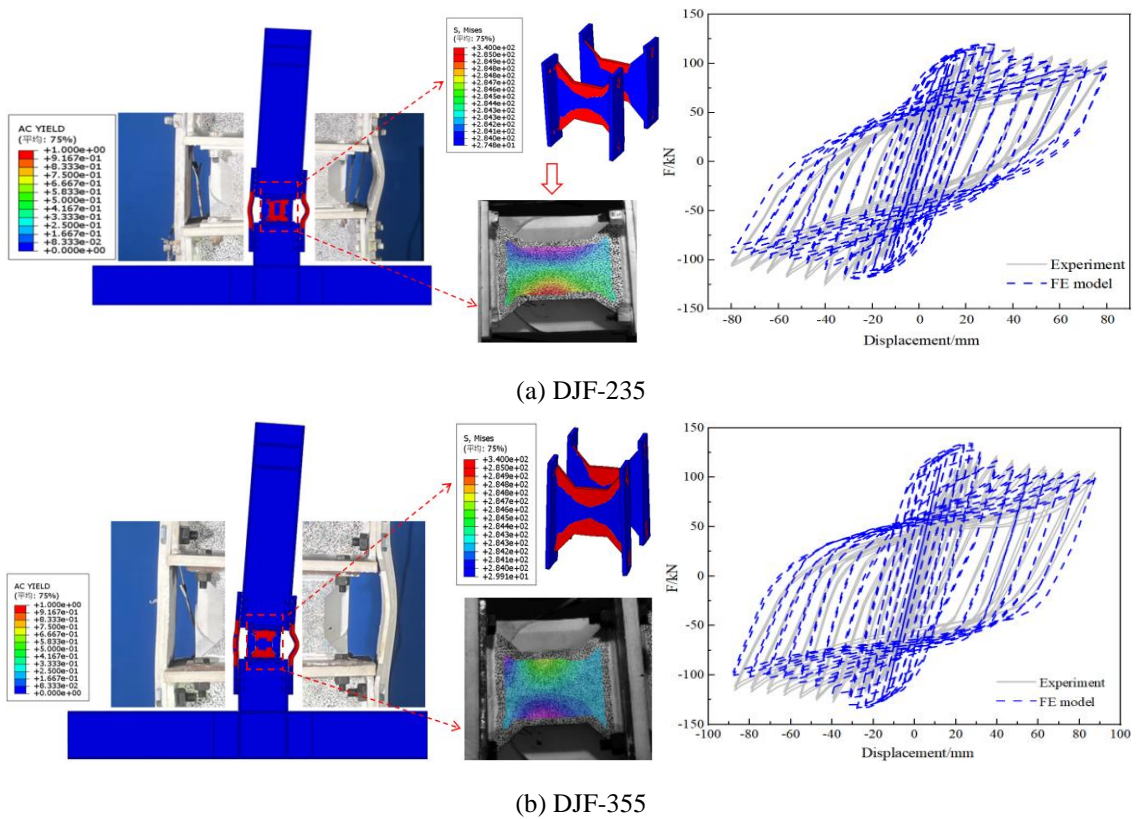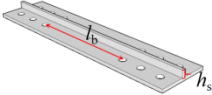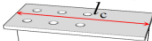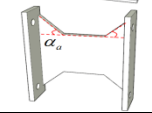

(a) DJF-235

(b) DJF-355

Fig. 12 Comparison of damage phenomena

5.2 Parameter expansion

From the experimental results, it can be concluded that the performance of damage element parameters as well as the cantilever beam can significantly affect the mechanical properties and damage modes of the joint. The effects of the length of the intermediate energy dissipation segments l_b of the flange cover plate, the height of the buckling-restraint rib of the flange cover plate h_s, the length of the cantilever beam l_c, and the cutting angle of the butterfly damper α_a on the performance of the joint were investigated. The specific parameter settings are shown in **Table 4**. Where P_m denotes the peak load carrying capacity and P_y denotes the yield load carrying capacity; K_m denotes the growth rate of peak load carrying capacity and K_y denotes the growth rate of yield load carrying capacity.

Table 4. Parameter setting of joint

	Variables	Original dimension	Parameter variation	Specimen number
	l_b	310(mm)	330/350/370	SL310-SL370
	h_s	20(mm)	10/30/40	SH10-SH40
	l_c	305(mm)	400/500/600	SC400-SC600
	α_a	45 °	50 °-60 °	SA50-SA60

(1) Parameter l_b

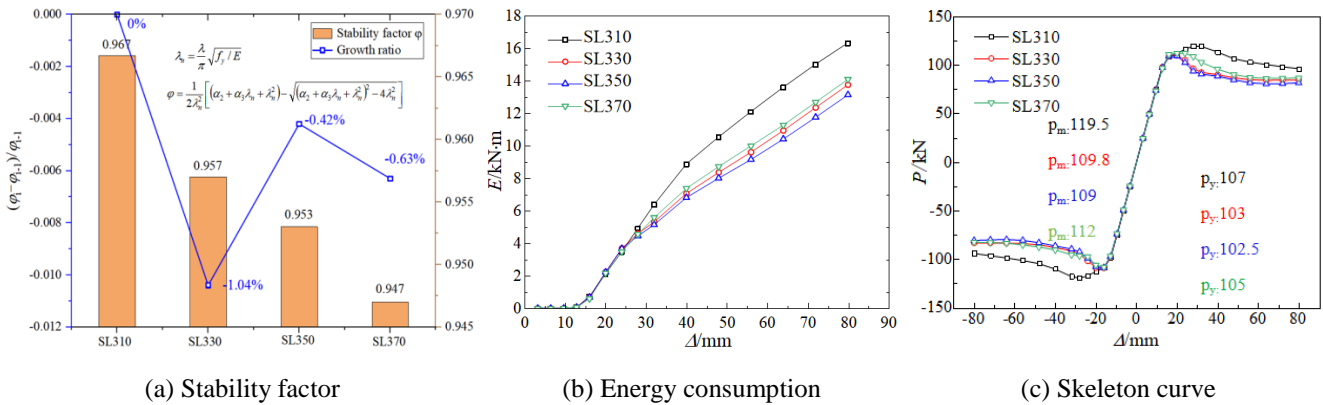| (a) Stability factor	(b) Energy consumption	(c) Skeleton curve

Fig. 13 Results of the analysis of the parameter l_b

The length of the intermediate energy dissipation segments of the flange cover plate can significantly affect its load stability. Four kinds of specimens SL310-370 were designed. The load capacity and energy dissipation capacity of the joints under the change of l_b parameter were investigated respectively, and the analyzed results are shown in **Fig. 13**. As shown in the figure, during the process of changing the length l_b of the energy dissipation section in the middle of the flange cover plate from 310mm to 370mm, the joint bearing capacity decreased by 8.8%, 9.6%, and 6.7% respectively. Additionally, the energy dissipation decreased by 18.9%, 24.4%, and 16.4% respectively. After calculation, the stability coefficient of the flange cover plate also decreased by 1.04%, 0.42%, and 0.63% respectively with the increase of the length of the middle energy dissipation section. The reason for the above is that as the length of the intermediate energy dissipation segments increases, it leads to a decrease in the stability coefficient of the flange cover plate, resulting in a buckling deformation of the flange cover plate before yielding. It can also be seen from **Fig. 14** that as the length of the intermediate energy dissipation segments increases, the plastic yield area of the flange cover plate gradually decreases, and the buckling deformation is gradually obvious. In summary, when designing the flange cover plate, it is important to consider the length of the intermediate energy dissipation segments. A longer length leads to a smaller stability coefficient, which is unfavorable for joint bearing performance.

When the stability coefficient is less than 0.967, both energy consumption and peak bearing capacity decrease significantly. As the stability coefficient continues to decline, joint energy consumption and bearing capacity tend to stabilize. Therefore, it is recommended to design the length of the intermediate energy dissipation segments of the flange cover plate to meet construction requirements and standard bolt spacing while ensuring that the stability coefficient is not less than 0.967.
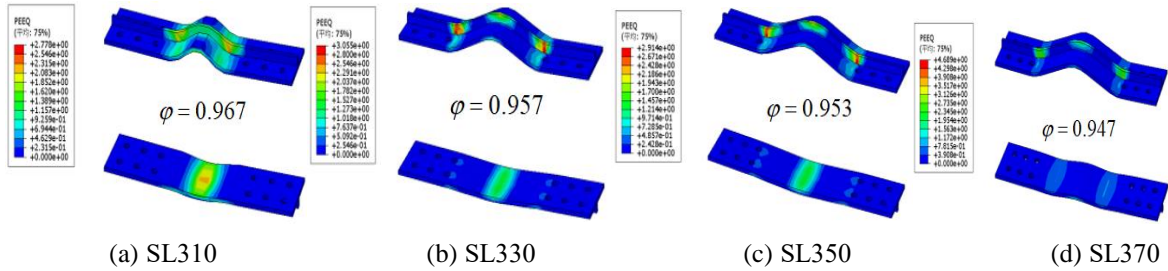

| (a) SL310 | (b) SL330 | (c) SL350 | (d) SL370 |

Fig. 14 Stress distribution

(2) Parameter h_s

A higher buckling-restraint rib of the flange cover plate is more favorable for the joint's load carrying capacity, but it may cause the cantilever beam to lose its elasticity. When designing earthquake-resistant joints, it is important to consider both the elasticity of beams and columns, as well as the bearing performance of the joints. The SH10-SH40 specimens for analysis, and the results are shown in (**Fig. 15, Fig. 16**). In the provided figure, it is observed that as the height of the buckling-restraint rib is increased from 10mm to 40mm, the joint bearing capacity shows growth ranges of 9.93%, 28.8%, and 9%, respectively. Additionally, the energy dissipation capacity exhibits growth ranges of 5.2%, 38%, and 16.8%, respectively. The data indicates that the maximum improvements in bearing capacity and energy dissipation are achieved when the height of the stiffeners is set to 30mm. It is suggested that the height of the buckling-restraint rib should be 0.2 times the width of the flange cover plate, considering its impact on joint performance and the main structure.
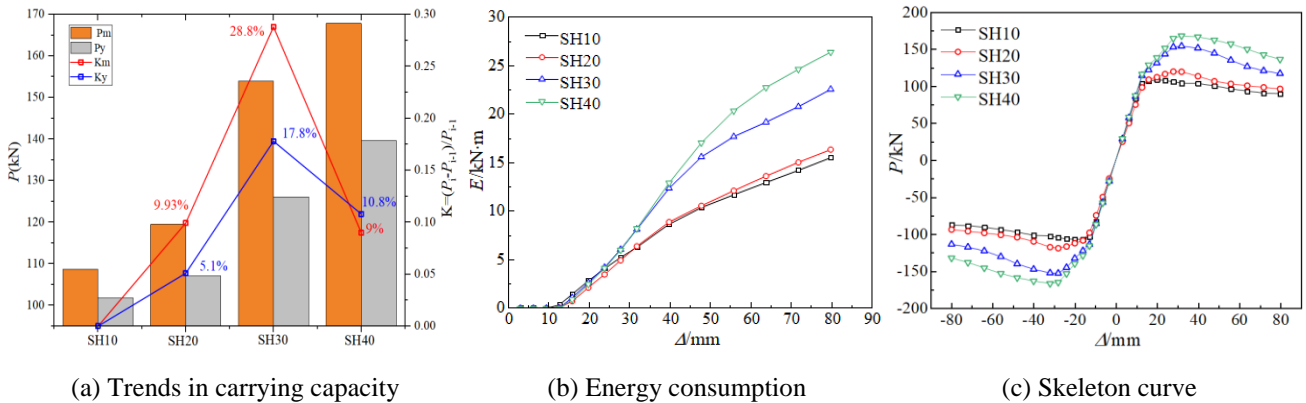

| (a) Trends in carrying capacity | (b) Energy consumption | (c) Skeleton curve |

Fig. 15 Results of the analysis of the parameter h_s

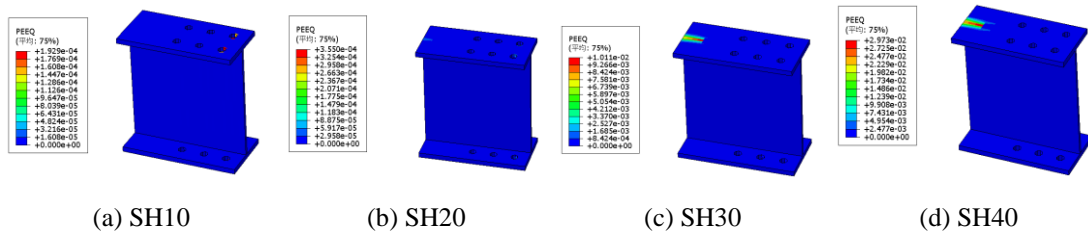| (a) SH10 | (b) SH20 | (c) SH30 | (d) SH40 |

Fig. 16 Stress distribution

(3) Parameter α_a

After finalizing the size design of the joint ear plate, the width L of the butterfly damper becomes

a fixed value. In this scenario, parameters H and L_1 are related to the cutting angle α_a of the butterfly damper. With this in mind, a specimen ranging from SA45 to SA60 was designed based solely on the cutting angle α_a. The analysis results are depicted in **(Fig. 17, Fig. 18)**. In the figure, when the cutting angle of the butterfly damper steel is increased from 45° to 60°, the joint bearing capacity increases by 15.6%, -0.2%, and -4% respectively. Likewise, the energy dissipation increases by 15.3%, 0%, and -5.8% respectively. When the cutting angle is set to 50°, the joint has its best load-bearing and energy dissipation capacity, and the level of damage to the butterfly damper is lower. If the angle is greater than 50°, the load-bearing capacity and energy consumption of the joint will decrease. When L is known, the relationship between H and L_1 can be obtained based on Equation 8 to design a butterfly damper.
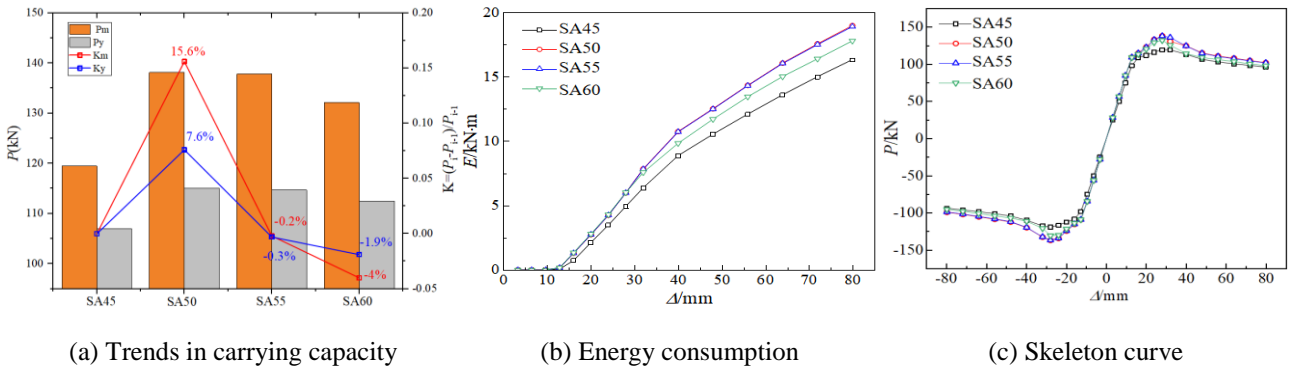
$$\tan \alpha_a = -2H/(L - L_1) \tag{8}$$

| (a) Trends in carrying capacity | (b) Energy consumption | (c) Skeleton curve |

Fig. 17 Results of the analysis of the parameter α_a

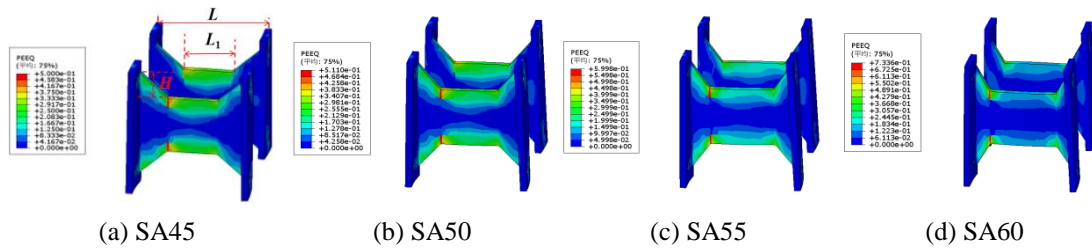| (a) SA45 | (b) SA50 | (c) SA55 | (d) SA60 |

Fig. 18 Stress distribution

(4) Parameter l_c

A series of specimens SC305-SC600 were designed to assess the length of the cantilever beam. The results of the analysis are shown in **(Fig. 19, Fig. 20)**. The figure indicates that as the length of the cantilever beam increased from 305mm to 600mm, the bearing capacity of the joint increased by 26%, 6%, and 10.3% respectively, and the energy dissipation increased by 22.6%, 2%, and 6.8% respectively. Longer cantilever beam lengths will also result in greater plastic damage at the connection of the beam and column. Considering the joint loading performance and the functional recovery performance after an earthquake, it is recommended that the length of the cantilever beam be 1.3 times the beam height.
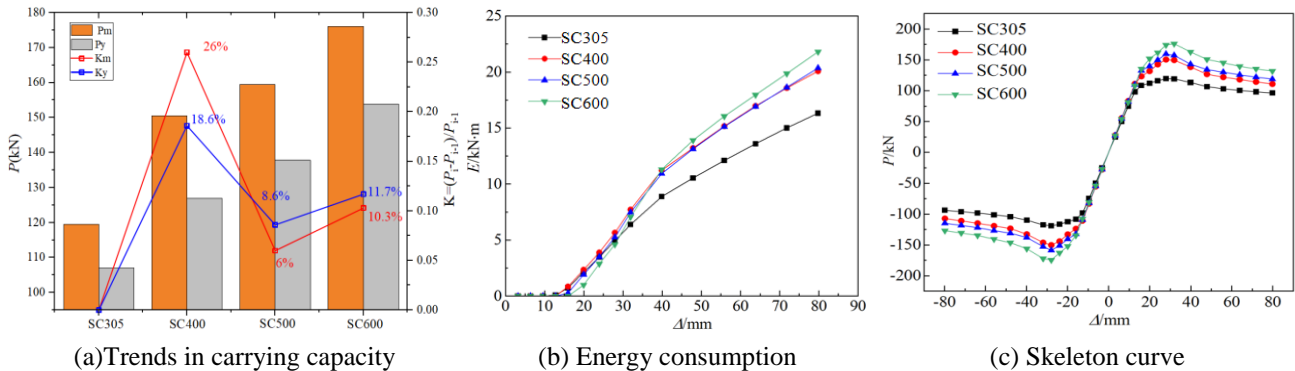

| (a)Trends in carrying capacity | (b) Energy consumption | (c) Skeleton curve |

Fig. 19 Results of the analysis of the parameter l_c

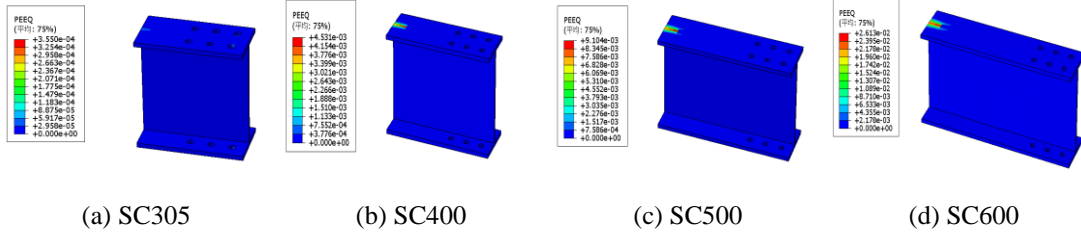(a) SC305   (b) SC400   (c) SC500   (d) SC600

Fig. 20 Stress distribution

According to the results of the joint parameter analysis, the joint damage element design method is summarized, and the results are shown in **Fig. 21**.
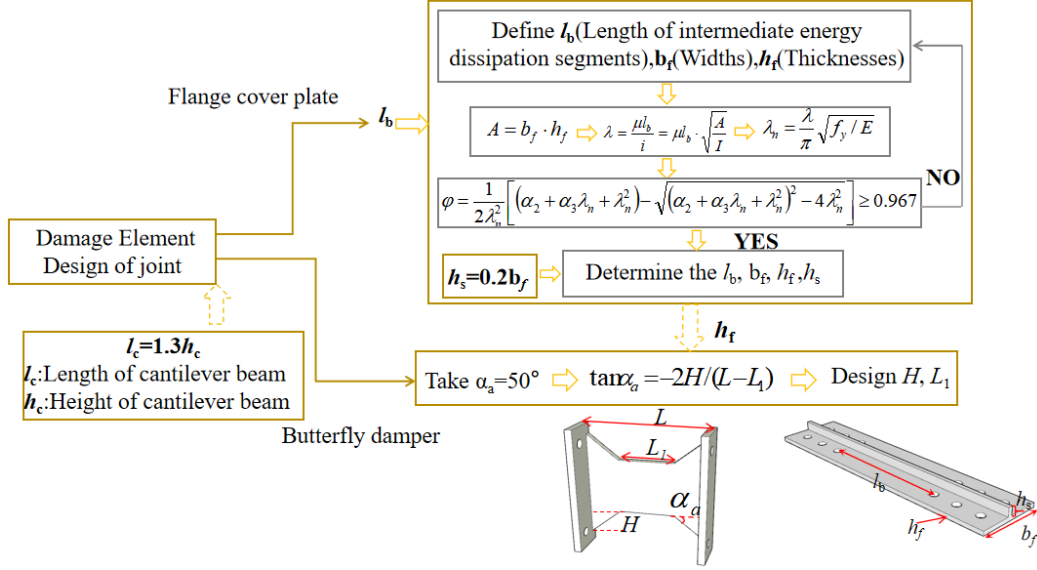

Fig. 21 Damage element design

6 Skeleton curve model

6.1 Bearing capacity of joint

The flange cover plate is crucial for bearing loads and dissipating energy before the joint yields. Therefore, the yield load of the joint only takes into account the impact of the flange cover plate. There are two yield modes for the flange cover plate: one is when the middle energy dissipation section of the flange cover plate reaches the yield strength, and the other is when the middle energy dissipation section of the flange cover plate buckles.

When the flange cover plate yields, the calculation formula is as Eq. (9-12), where l_p is the distance from the beam loading end to the center of the splicing section, taken as 1360mm; other parameters are detailed in **Fig. 22**.

$$A = B \cdot h - (B - b) \cdot (h - c) \tag{9}$$

$$I_{flange} = \frac{1}{3}\left[(B-b)c^3 + bh^3\right] - e_{y'}^2 A \tag{10}$$

$$I_{b,flange} = \frac{1}{3}\left[(B-b)c^3 + bh^3\right] - e_{y'}^2 A + (e_y' + \frac{h_b}{2})^2 \cdot A \tag{11}$$

$$F_y = \frac{f_y I_{b,flange}}{(e_y' + h_b/2) \cdot l_p} \tag{12}$$

When the flange cover plate buckles, the formula for calculating the bearing capacity is shown in

Eq. (13-15). In the equation, λ_n is the regularized aspect ratio of the flange cover plate, and ϕ is the stability coefficient of the flange cover plate. F_y and E are the yield strength and elastic modulus of the steel, respectively.
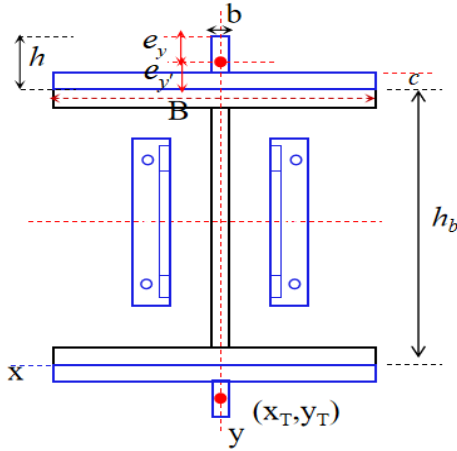

Fig. 22 Section size of joint

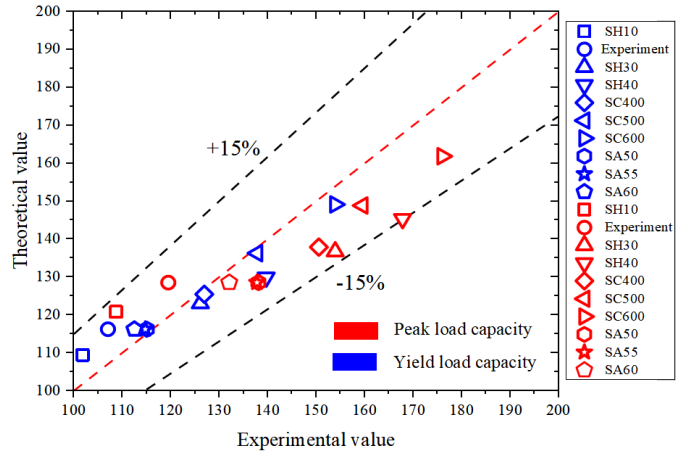**Fig. 23** Calculation results of joint bearing capacity

$$\lambda_n = \frac{\lambda}{\pi}\sqrt{f_y / E}$$

(13)

当 $\lambda_n \leq 0.215$：

$$\phi = 1 - \alpha_1 \lambda_n^2$$

(14)

当 $\lambda_n > 0.215$：

$$\phi = \frac{1}{2\lambda_n^2}\left[\left(\alpha_2 + \alpha_3\lambda_n + \lambda_n^2\right) - \sqrt{\left(\alpha_2 + \alpha_3\lambda_n + \lambda_n^2\right)^2 - 4\lambda_n^2}\right]$$

(15)

After calculation, $\lambda_n = 0.32$. According to the specification GB50017-2017, the section type of the flange cover plate belongs to class b, so $\alpha_1 = 0.65$, $\alpha_2 = 0.965$，$\alpha_3 = 0.3$. By substituting it into Eq. (15), it can be obtained that $\phi = 0.944$. By substituting the value into Eq. (16), F_s can be obtained. Finally, the smaller value of F_y and F_s is taken as the yield bearing capacity of the joint, as shown in Eq. (17).

$$F_s = \phi A_{cov} f_y (y_T + h_b) / l_p$$

(16)

$$F = \min(F_y, F_s)$$

(17)

The peak load considers the contribution of butterfly dampers to the bearing capacity of joints, and the calculation formula for the peak load of joint is shown in Eq. (18), where W_p is the plastic section modulus.

$$F_p = f_y \cdot W_p / l_p$$

(18)

To validate the accuracy of the joint loading capacity calculation method, the theoretical calculations with experimental and finite element simulation results are compared. The findings are presented in **Fig. 23**. Based on the data in **Fig. 23,** the variance between the calculated and experimental results for the joint's bearing capacity is within 15%. This confirms the efficacy of the calculation method for assessing the bearing capacity of beam-column joints with doubly damaged elements.

6.2 Initial stiffness calculation model

The stiffness calculation is divided into two parts: the bending stiffness of the flange cover plate and the shear stiffness of the butterfly damper. The schematic diagram for calculating the bending stiffness of the flange cover plate is shown in **Fig. 24**. In the diagram, l, E, and I represent the length of the energy dissipation section in the middle of the flange cover plate, the elastic modulus, and the section moment of inertia, respectively. When subjected to load F, the flexibility equation of the flange cover plate is shown in Eq. (19).

$$y(x) = \frac{Fl^3}{6EI}(2 - \frac{3x}{l} + \frac{x^3}{l^3})$$

(19)

Assuming that the flange cover plate is bent and deformed at the center position, taking x=l/2, the stiffness expression is shown in Eq. (20):

$$K_F = \frac{48EI}{5l^3}$$

(20)

Under the action of bending moment M_0, the flexibility equation is shown in Eq. (21).

$$y(x) = -\frac{M_0 l^2}{2EI}\left(1 - \frac{x}{l}\right)^2$$

(21)

If x=l/2, the stiffness expression is $K_{M0} = 8EI / (L_0 l^2)$, and the bending stiffness of the flange cover plate can be obtained as Eq. (22):

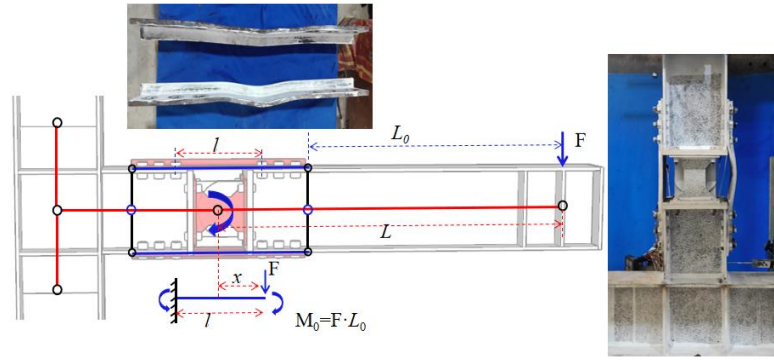$$K_{bending} = K_F + K_{M0}$$

(22)

Fig. 24 Calculation of stiffness of flange cover plate

The butterfly damper undergoes shear deformation and bending deformation of the connecting plate during the loading process, so the stiffness is also divided into two parts, namely shear stiffness and bending stiffness of the connecting plate. The force schematic diagram is shown in **Fig. 25**, where G and t are the shear modulus of the steel and the thickness of the butterfly damper, respectively. The expression for shear deflection of butterfly dampers is shown in Eq. (23):

$$y_{shear} = \frac{Fl_1}{GA_1} + \frac{Fl_2}{GA_2}$$

(23)

$$A_1 = h_d t$$

(24)

$$A_2 = (h_d + l_2 / 2 \cdot \tan \theta)t$$

(25)

The shear stiffness of the butterfly damper is shown in Eq. (26):

$$K_{shear} = \frac{GA_1}{l_1} + \frac{GA_2}{l_2}$$

(26)

According to the calculation method of the bending stiffness of the flange cover plate, the expression for the bending stiffness of the butterfly damper connecting plate can be obtained as Eq. (27), where I_2 is the cross-sectional moment of inertia of the connecting plate, and l_3 is the distance from the center of the bolt hole to the end of the connecting plate.

$$K_{d,c} = 3EI_2 / l_3^3$$

(27)

The expression for the initial rotational stiffness of the node is shown in Eq. (28):

$$K_0 = \frac{1}{\dfrac{1}{2K_{bending}} + \dfrac{1}{2K_{sheear}} + \dfrac{1}{2K_{d,c}}}$$

(28)

To assess the accuracy of the initial stiffness calculation method for the joint, we compared the

theoretical calculation results with experimental and finite element simulation results. The findings are presented in **Fig. 26.** As shown in the figure, the error between the calculated initial stiffness of the joint and the experimental results is within 10%. This confirms the effectiveness of the calculation method for the initial stiffness of beam column joint with double damage elements.
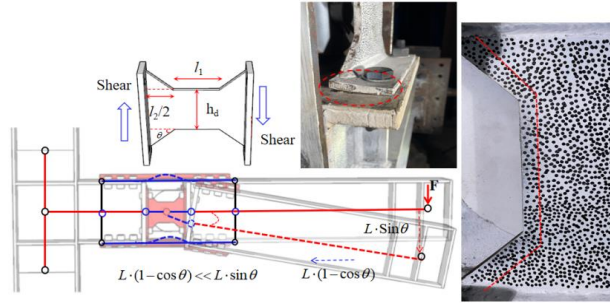

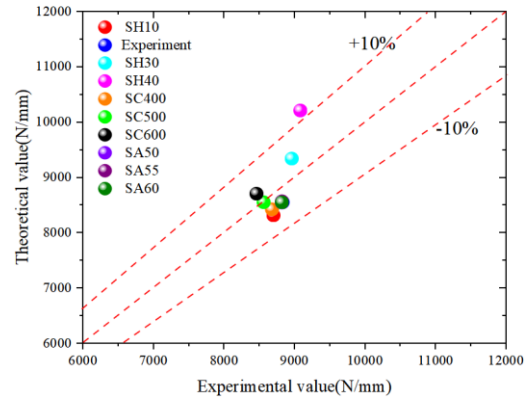Fig. 25 Calculation of stiffness for butterfly dampers

Fig. 26 Initial stiffness calculation results

The yield and peak load capacity of the joint are calculated using Eq. (17, 18) in section 5.1. The initial joint stiffness is determined using Eq. (27) in section 5.2. At this point, most of the skeleton curves around the structure are solved using a combination of theory and data fitting [32]. During the process of solving the skeleton curve, it is established that the curve has a trilinear characteristic by fitting the data from each stage of the curve. The coordinates of the yield point (u_y, F_y) are determined by calculating the yield capacity in section 5.1 and the initial stiffness K_0 in section 5.2. This stage is completed through theoretical calculations. In the second step, the linear expressions for the elastic, strengthening and degraded segments of the skeleton curve are obtained by curve fitting as shown in Eq.(29-31). On this basis, the relationship between the stiffness of the skeleton curve in the strengthening stage and the degradation stage and the initial stiffness K_0 can be obtained, i.e., $K_{AB}=0.087K_0$, $K_{BC}=-0.064K_0$. The fitting of each stage of the skeleton curve is shown in **Fig. 27**.

Elastic segment:

$$P / P_{max} = 1.567(\Delta / \Delta_{max})$$
(29)

Reinforcement segment:

$$P / P_{max} = 0.136(\Delta / \Delta_{max}) + 0.684$$
(30)

Degradation segment:

$$P / P_{max} = -0.1(\Delta / \Delta_{max}) + 1.1$$
(31)

Finally, the peak point coordinates (u_k, F_k) of the skeleton curve can be found using K_{AB}, along with the peak load capacity calculated in section 5.1. The extreme point coordinates (u_u, F_u) of the skeleton curve can be determined using K_{BC} and combined with the ultimate displacement of the joint. The calculation procedure of the joint skeleton curve is shown in **Fig. 28**.
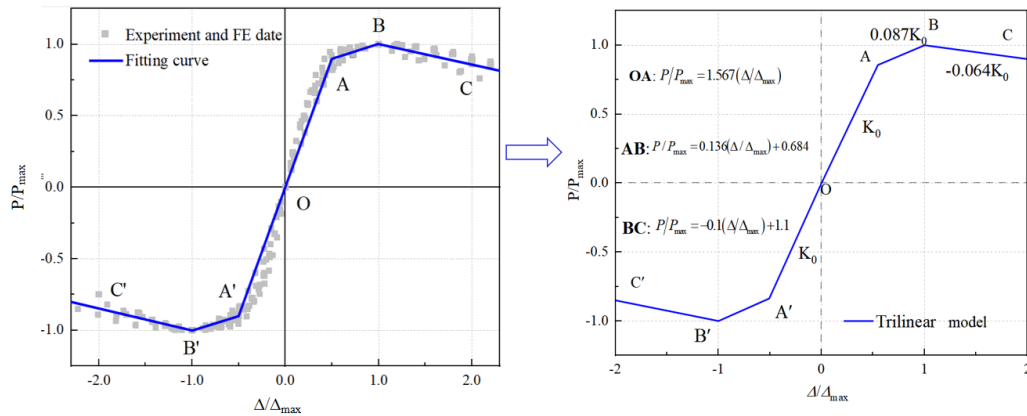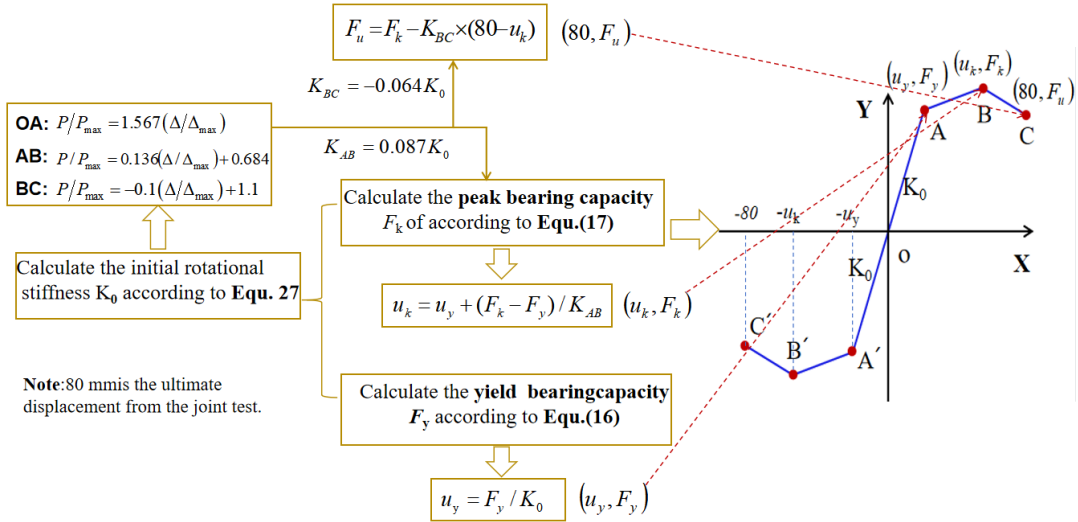

Fig. 27 Skeleton curve fitting

Fig. 28 Calculation process of skeleton curve

Six specimens, SH20 (Experiment), SH30, SC400, SC500, SA50, and SA60, were selected to compare the theoretical calculation results of the skeleton curve with the experimental and finite element results, as shown in **Fig. 29**. It can be seen from **Fig. 29** that the theoretical calculation results of the skeleton curve are in good agreement with the experimental and finite element calculation results, indicating that the skeleton curve model can accurately reflect the mechanical properties of the recoverable nodes of high-strength steel with double damage after earthquakes.
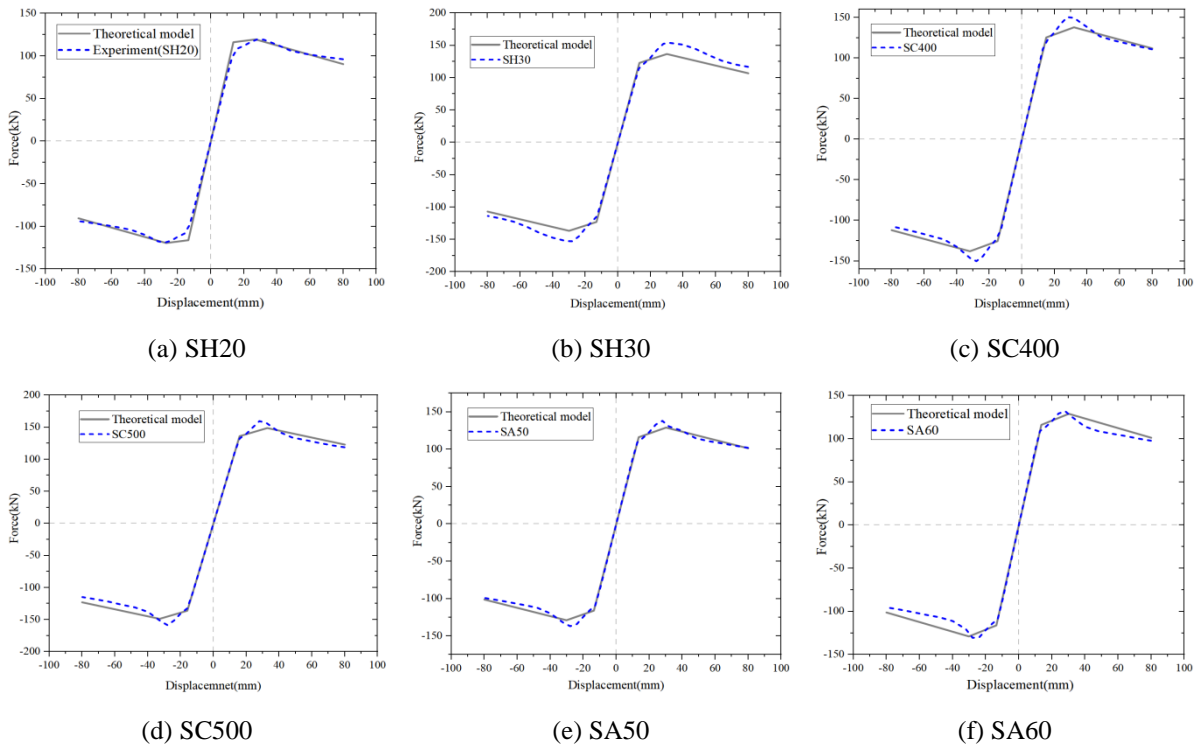

(a) SH20   (b) SH30   (c) SC400

(d) SC500   (e) SA50   (f) SA60

Fig. 29 Validation of skeleton curve model

7 Conclusion

Through the analysis, the following conclusions can be obtained:

(1)Through experiments, it was discovered that there is a significant time sequence phenomenon in the yield between the flange cover plate and the butterfly damper. The energy dissipation ratio of both exceeds 90%, while the energy dissipation ratio of the beam column main component is less than

10%. Upon calculation, it was determined that the residual deformation of the joints is lower than the DS2 level limit specified in the FEMA P-58 standard. This indicates that the joints have excellent post-earthquake recoverability performance, and the damage element can effectively protect the beams and columns from damage.

(2)After replacing the damaged steel material from Q235 to Q355, the joint's yield displacement increased by 27%, the yield load increased by 10.7%, and the energy dissipation increased by 54.8%. However, the ductility and peak bearing capacity remained basically unchanged. A comprehensive analysis shows that the strength of damaged steel significantly affects the energy dissipation and yield load of joints, but further research is needed to understand its impact on ductility and peak load.

(3)After analyzing various parameters, it was determined that the length (lb) of the energy dissipation section in the middle of the flange cover plate determines its aspect ratio, which in turn influences the loading stability of the flange cover plate. Considering all factors, it is recommended that the stability coefficient of the flange cover plate design should be no less than 0.967. The length of the cantilever beam should be 1.3 times its cross-sectional height, the height of the buckling restraint rib of the flange cover plate should be 0.2 times its width, and the cutting angle of the butterfly damper should be set at 50°.

(4) A calculation method for the joint trilinear skeleton model has been proposed based on theoretical derivation and data fitting. The calculation steps for the skeleton curve model have been outlined. By comparing the theoretical calculation results with experimental and finite element results, it was found that the curves were in good agreement. This proves the effectiveness of the proposed joint skeleton curve model calculation method and can provide a theoretical reference and basis for the calculation of similar structural skeleton models.

(5) This article examines the seismic performance of high-strength steel beam-column joints with double damage elements. However, it does not mention the seismic performance of this type of structural system and how it compares to traditional steel frames. Subsequent research will analyze and discuss the high-strength steel frame structure system with double damage elements to provide new ideas for promoting and applying earthquake-resilient structures.

Acknowledgement

CRediT authorship contribution statement

Hongchao Guo: Investigation, Methodology, Funding acquisition, Writing-review & editing, Supervision. **Dongdong Zheng:** Data analysis & processing, Writing-original draft, Writing-review & editing, calculating method, Visualization. **Jing Lu:** Numerical simulation, & editing. **Xu dong Zhou:** Numerical simulation, & editing. **Wenqi Wang:** Numerical simulation, & editing. **Yunhe Liu:** Formal analysis, & editing.

Conflicts of Interest

All the authors do not have any possible conflicts of interest.

References

[1] S.A. Mahin, Lessons from damage to steel buildings during the Northridge earthquake. Eng. Struct,1998; 20(4): 261-270. https://doi.org/10.1016/S0141-0296(97)00032-1.

[2] M. Nakashima, K. Inoue, M. Tada, Classification of damage to steel buildings observed in the 1995 Hyogoken-Nanbu earthquake. Eng. Struct 1998; 20(4) :271-281. https://doi.org/10.1016/S0141-0296(97)00019-9.

[3] C.E. Sofias, D.T. Pachoumis. Assessment of reduced beam section (RBS) moment connections subjected to cyclic loading. Journal of Constructional Steel Research 2020; 171:106151. https://doi.org/10.1016/j.jcsr.2020.106151.

[4] Hongchao Guo, Kuanhong Mao, Jinguang Yu, et al. Experimental and numerical study on seismic

performance plate-reinforced and tapered-reduced composite joints. Structures 2021; 31:686-707. https://doi.org/10.1016/j.istruc.2021.01.087.

[5]   Gang liang, Zhihan Lu, Hongchao Guo, et al. Experimental and numerical investigation on seismicperformance of extended stiffened end-plate joints with reduced beam section using high strength steel.Thin-Walled Structures 2021; 169: 108434. https://doi.org/10.1016/j.tws.2021.108434.

[6]   Chen C, Qiao H, Wang J. Chen Y. Progressive collapse behavior of joints in steel moment frames involving reduced beam section. Engineering Structures 2020; 225: 111297. https://doi.org/10.1016/j.engstruct. 2020. 111297.

[7]   Qiao H，Chen Y，Wang J, Chen C. Experimental study on beam-to-column connections with reduced beam section against progressive collapse. Journal of Constructional Steel Research 2020;175: 106358. https://doi. org/10.1016/j.jcsr.2020.106358.

[8]   Quanming Yang, Huiyong Ban. Balanced design philosophy of superior high-performance steel cover-plated beam-to-column joints. Thin-Walled Structures 2023; 184: 110470. https://doi.org/10.1016/j. tws.2022.110470.

[9]   Hongchao Guo, Xizhe Zhou, Wei Li, et al. Experimental and numerical study on seismic performance of Q690 high-strength steel plate reinforced joints. Thin-Walled Structures 2021; 161: 107510. https://doi.org/10.1016/j.tws.2021.107510.

[10]   Ai-Lin Zhang, Ping Qiu, Kang Guo, et al. Experimental study of earthquake-resilient end-plate type prefabricated steel frame beam-column joint. Journal of Constructional Steel Research 2020; 166: 105927. https://doi.org/10.1016/j.istruc.2023.02.063.

[11]   Zi-qin Jiang, Yi-Tao Kang, Xue-Chun Liu, et al. Experimental study of an earthquake-resilient prefabricated opening-web steel channel beam-to-column joint with flange cover plates. Engineering Structures 2020; 221: 111054. https://doi.org/10.1016/j.engstruct.2020.111054.

[12]   Antonella B. Francavilla, Massimo Latour, Gianvittorio Rizzano, et al. Experimental assessment of the hysteretic response of resilient low-damage friction joints with different Belleville disk springs configurations. Soil Dynamics and Earthquake Engineering 2024; 180: 108617. https://doi.org/10.1016/j.soildyn.2024.108617.

[13]   Zhi-an Jiao, Lin-zhao Cui, Hang-hang Liu, et al. Design and numerical analysis of new earthquake-resilient semi-rigid joints. Journal of Constructional Steel Research 2024; 213: 108393. https://doi.org/10.1016/j.jcsr.2023.108393.

[14]   Jinjie Men, Tong Li, Qi Zhou, et al. Structural fuse performance and earthquake-resilient performance of beam-column joints with replaceable T-stub. Journal of Constructional Steel Research 2023; 206: 107943. https://doi.org/10.1016/j.jcsr.2023.107943.

[15]   Ge Zhang, Longhe Xu, Xingsi Xie, et al. Seismic evaluation of a self-centering retrofit solution for modular steel structure connections. Journal of Constructional Steel Research 2024; 218: 108701. https://doi.org/10.1016/j.jcsr.2024.108701.

[16]   Ruyue Liu, Yunzhao Zhu, Guiyun Yan,etal. Behavior of the damage-tolerant beam-column connectio n for earthquake-resilient steel frame: Experimental and numerical study. Structures 2024; 67: 106985. https://doi.org/10.1016/j.istruc.2024.106985.

[17]   Ying-lu Xu, Yao-xuan Su, Yong-fang Shang, etal. Seismic performance of earthquake-resilient prefabri cated corrugated web beam-column connection with buckling-restrained plates. Journal of Construction al Steel Research 2022; 194: 107327. https://doi.org/10.1016/j.jcsr.2022.107327.

[18]   Yong chao Guo, Meng Wang. Experimental study on mechanical behavior and resilient performance of steel frame connection with low-yield-point steel fuses. Engineering Structures 2022; 266: 114599. https://doi.org/10.1016/j.engstruct.2022.114599.

[19]   Lewei Tong, Yingzhi Chen, Yiyi Chen, et al. Cyclic behaviour of beam-to-column joints with cast steel connectors. Journal of Constructional Steel Research 2016; 116: 114-130. https://doi.org/10.1016/j. jcsr.2015.09.005.

[20]   McCormick J, Aburano H, Ikenaga M, et al．Permissible residual deformation levels for building structures considering both safety and human elements[C]//Proceedings of the 14th World Conference on Earthquake Engineering. Harbin, China: Chinese Association of Earthquake Engineering,2008: 12-17.

[21]   McCormick D, Aburano H, Ikenaga M, et al. Permissible residual deformation level for building structures considering both safety and human elements [C]. Proc.14th World Conf. Earthquake Engng, Beijing, China, Paper No. 05-06-0071, 2008.

[22]   Erochko J, Christopoulos C, Tremblay R, et al. Residual drift response of SMRF and BRB frames in steel buildings according to ASCE 7-05. Journal of Structural Engineering 2011; 137: 589-599. DOI: 10.1061/(ASCE)ST.1943-541X.0000296.

[23]   ANSI/AISC 341-16. Seismic provisions for structural steel buildings. Chicago: American Institute of Steel Construction. 2016.

[24] EN 1998-1:2004. Eurocode 8-Design of structures for earthquake resistance-part 1: General rules, seismic actions and rules for buildings. Brussels: European Committee for Standardization. 2004.

[25] SAC Joint Venture. FEMA-267 Report No. SAC-95-02 Interim guidelines: Evaluation, repair, modification and design of steel moment frames. Federal Emergency Management Agency. 1995.

[26] ANSI/AISC 341-10, Seismic Provisions of Structural Steel Buildings, American Institute of Steel Construction, Chicago, USA; 2010.

[27] GB/T228.1-2021, Metallic Materials-Tensile Testing Part 1: Method of test at room temperature, China Standard Press, Beijing, 2021 (in Chinese).

[28] ECCS. Recommended testing procedure for assessing the behaviour of structural steel elements under cyclic loads. 1986.

[29] Shen Li, Qi Ding, Hongchao Guo, et al. Experimental study on seismic performance of two-segment replaceable link with separated splicing plates. Journal of Constructional Steel Research 2024; 213: 108413. https://doi.org/10.1016/j.jcsr.2023.108413.

[30] Ai-Lin Zhang, Xiang-Yuan Li , Zi-Qin Jiang, et al. Experimental study of earthquake-resilient prefabricated composite joint with T-shape connector. Journal of Constructional Steel Research 2021; 184: 106831. https://doi.org/10.1016/j.jcsr.2021.106831.

[31] Federal Emergency Management Agency (FEAM) .Seismic performance assessment of buildings: volume 1: methodology: FEMA P-58-1[S].Washington D C: Federal emergency Management Agency, 2012.

[32] ZHANG Yue, LI Dongsheng. Restoring force model of precast concrete-filled steel tube column-to-RC beam connections with energy-dissipating bolts. Journal of Building Structures 2023; 44(4): 309-318. DOI:10.14006/j.jzjgxb.2020.0557.